Atmos. Chem. Phys., 15, 1707–1724, 2015
www.atmos-chem-phys.net/15/1707/2015/
doi:10.5194/acp-15-1707-2015

Atmospheric Chemistry and Physics
Open Access

An attempt at estimating Paris area CO_2 emissions from atmospheric concentration measurements

F. M. Bréon[1], G. Broquet[1], V. Puygrenier[1], F. Chevallier[1], I. Xueref-Remy[1], M. Ramonet[1], E. Dieudonné[1], M. Lopez[1], M. Schmidt[1], O. Perrussel[2], and P. Ciais[1]

[1]Laboratoire des Sciences du Climat et de l'Environnement, UMR CEA-CNRS-UVSQ, Gif sur Yvette, France
[2]AirParif, 7 rue Crillon, Paris, France

Correspondence to: F. M. Bréon (breon@lsce.ipsl.fr)

Received: 22 January 2014 – Published in Atmos. Chem. Phys. Discuss.: 10 April 2014
Revised: 20 January 2015 – Accepted: 27 January 2015 – Published: 18 February 2015

Abstract. Atmospheric concentration measurements are used to adjust the daily to monthly budget of fossil fuel CO_2 emissions of the Paris urban area from the prior estimates established by the Airparif local air quality agency. Five atmospheric monitoring sites are available, including one at the top of the Eiffel Tower. The atmospheric inversion is based on a Bayesian approach, and relies on an atmospheric transport model with a spatial resolution of 2 km with boundary conditions from a global coarse grid transport model. The inversion adjusts prior knowledge about the anthropogenic and biogenic CO_2 fluxes from the Airparif inventory and an ecosystem model, respectively, with corrections at a temporal resolution of 6 h, while keeping the spatial distribution from the emission inventory. These corrections are based on assumptions regarding the temporal autocorrelation of prior emissions uncertainties within the daily cycle, and from day to day.

The comparison of the measurements against the atmospheric transport simulation driven by the a priori CO_2 surface fluxes shows significant differences upwind of the Paris urban area, which suggests a large and uncertain contribution from distant sources and sinks to the CO_2 concentration variability. This contribution advocates that the inversion should aim at minimising model–data misfits in upwind–downwind gradients rather than misfits in mole fractions at individual sites. Another conclusion of the direct model–measurement comparison is that the CO_2 variability at the top of the Eiffel Tower is large and poorly represented by the model for most wind speeds and directions. The model's inability to reproduce the CO_2 variability at the heart of the city makes such measurements ill-suited for the inversion. This and the need to constrain the budgets for the whole city suggests the assimilation of upwind–downwind mole fraction gradients between sites at the edge of the urban area only.

The inversion significantly improves the agreement between measured and modelled concentration gradients. Realistic emissions are retrieved for two 30-day periods and suggest a significant overestimate by the AirParif inventory. Similar inversions over longer periods are necessary for a proper evaluation of the optimised CO_2 emissions against independent data.

1 Introduction

Although the total CO_2 emissions of developed countries may be well constrained from the total consumption of fossil fuel, their spatial and temporal distribution are not known with the same level of accuracy. In so-called bottom-up emission estimates, CO_2 emission is calculated as a combination of geo-referenced activity proxies (e.g. road traffic data, or number and type of buildings that relate to residential emissions; Gurney et al., 2012) multiplied by emission factors, accounting for the disaggregation of national annual budgets when dealing with regional or city inventories. The accuracy of the bottom-up inventories is seldom assessed and mostly relies on the difference between various estimates and on expert knowledge.

Due to the high population density associated with ground transportation, residence and industry, anthropogenic CO_2 emissions are large within cities (Pataki et al., 2006). The emitted CO_2 is transported in the atmosphere and results in

elevated CO_2 concentration above and downwind of cities. There is therefore a potential to estimate the net CO_2 flux of a city from a few atmospheric concentration measurements located within or in the vicinity of the city (McKain et al., 2012). Over a very dense urban area, the net CO_2 flux is dominated by fossil fuel emissions, but over less dense urban structures, the net ecosystem exchange (NEE) becomes significant and can partly offset fossil CO_2 emissions during the growing season (Nordbo et al., 2012). Top-down net CO_2 flux estimates, constrained by independent atmospheric measurements, could come in complement to, or for the assessment of, current estimates that rely on bottom-up inventories.

The technique of estimating surface CO_2 fluxes from atmospheric composition measurements – and potentially from prior information – is relatively mature. It has been used for many years to estimate the biogenic fluxes on the global (Gurney et al., 2002; Chevallier et al., 2010), continental (Broquet et al., 2013; Peylin et al., 2005) and regional (Lauvaux et al., 2009, 2012) scales. However, because of uncertainties in the atmospheric transport, insufficient measurement sampling, and inconsistencies between the mathematical framework hypothesis of most inversions (e.g. no biases, Gaussian distribution of errors, uncorrelated observation errors) and the reality, the results are not always consistent, in particular on the regional scale, as shown for instance through the recent comparison of global- and continental-scale biogenic flux estimates by several global inversions (Peylin et al., 2013).

Estimating the net CO_2 flux of a city using similar mathematical and modelling tools amplifies the difficulties inherent to the atmospheric inversion. The spatial heterogeneity of the source and the possibility of having very high emissions locally (e.g. a power plant) make the structure of the prior error statistics complex and the concentration plume highly variable. Relating mole fractions to city sources furthermore requires accurate atmospheric transport modelling on a fine scale. Atmospheric transport in urban areas is influenced by specific meteorological processes such as higher roughness of urban canopies (Zhao et al., 2014) and urban heat island effects (Nehrkorn et al., 2013). For instance, Pal et al. (2012) reported significantly thicker boundary layer over the city of Paris than in the surrounding rural area during a 4-day campaign that took place in March 2011, which was interpreted as a consequence of the urban heat island effect. Another difficulty, shared with the inversion of biogenic fluxes, lay in the temporal variability of the fossil fuel emissions, which have a strong daily cycle but also day-to-day variability resulting from, for instance, temperature changes (through heating) or activity (e.g. traffic) variability. Last, measurements in and around a target city collect CO_2 molecules of various origins that must be separated into city sources and remote sources and sinks through the inversion.

This challenge has been addressed recently by several research projects, e.g. INFLUX (sites.psu.edu/influx; Turnbull et al., 2014) over Indianapolis or Megacities (http://megacities.jpl.nasa.gov; Duren and Miller, 2012) over Los Angeles, which have set up a network of surface, tower and airborne measurements of the atmospheric CO_2 mole fractions. Satellite data may also provide valuable information as shown by Kort et al. (2012). The results from the ongoing urban CO_2 measurement project at Salt Lake City indicated that monthly emission relative changes of 15 % could be detected at the 95 % confidence level with the current monitoring system (McKain et al., 2012) even though this study concluded on the inability to derive absolute estimates for a given month.

The CO_2-Megaparis project has a similar objective for the Paris area. This is a potentially favourable case as the city is very dense and the emissions intense over a limited surface, with a fairly flat topography in the surroundings, which makes the atmospheric transport modelling easier. A pilot campaign in early 2010 was conducted in the framework of the MEGAPOLI project. Measurements of the mole fraction of CO_2 and its isotopes have been used to estimate the relative contribution of fossil and biogenic emissions in the concentration gradients (Lopez et al., 2013). The main campaign started in August 2010 with the installation of three CO_2 and CO monitoring stations within the city and its surroundings that provided near-continuous measurements until July 2011. These three stations complement two stations of the ICOS France network located in the Paris region outside the city that have been operational for several years. Lac et al. (2013) made a first analysis of the measurements and a comparison against atmospheric modelling using the Meso-NH mesoscale transport model, combined with a surface scheme that accounts for the urban environment, for a period of 5 days in March 2011. They demonstrated the ability of the modelling framework to reproduce several features of the mixing layer height, as reported in Pal et al. (2012), and of the mole fraction daily cycle.

Large efforts have been made by AirParif, the air quality agency for the Paris area, to generate an inventory of the Paris area emissions, for various pollutants and for CO_2 as well. The AirParif emission inventory, detailed in Sect. 2.2, provides an hourly description of the CO_2 emissions at $\approx$1 km resolution for representative weekdays and months. We use this inventory as an input to the atmospheric transport simulations and compare the results to the atmospheric concentration measurements from the five sites. We then attempt a correction of the inventory based on the differences between the observed and modelled mole fractions. With only five stations in the vicinity of the city, there is likely not enough information to constrain the spatial distribution of the emissions. We therefore only rescale the emissions, relying on the spatial distribution provided by the Airparif inventory. For the inversion, NEE and fossil fuel emissions are optimised separately. We focus on two 30-day periods in the autumn of 2010. This choice is driven by the expectation of rather small biogenic fluxes during this time period, which makes easier the interpretation of the measurements in terms

Table 1. Information about the CO_2 measuring stations that are used in this paper.

Location	Acronym	Latitude (°)	Longitude (°)	Height a.g.l. (m)	Distance from Paris centre (km)
Eiffel Tower	EIF	48.8582	2.2946	300	4 (W)
Montgé-en-Goële	MON	49.0284	2.7489	9	35 (NE)
Gonesse	GON	48.9908	2.4446	4	16 (N)
Gif-sur-Yvette	GIF	48.7100	2.1475	7	23 (SW)
Trainou forest	TRN	47.9647	2.1125	180	101 (S)

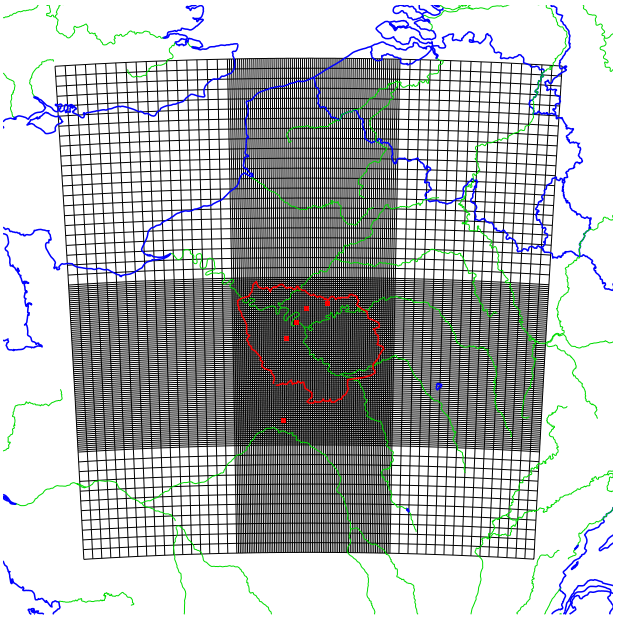

Figure 1. Map of the study area showing the location of the continuous CO_2 measurement stations that are used in this paper (red dots). The black lines show the model grid with a 2 km resolution at the centre, and 10 km on the sides. The red line shows the limits of the Île-de-France region.

of anthropogenic fluxes. Our objective is to assess whether a reliable estimate of the emissions on the daily to monthly timescales can be derived from the combination of atmospheric measurements, available inventories and information on the atmospheric transport. A forthcoming paper will apply the methodology to a full year of observations and analyse the result for the spring and summer periods, when CO_2 uptake by NEE can partially offset fossil fuel emissions (Pataki et al., 2007). In the following, Sect. 2 analyses the time series of measured and modelled CO_2 mole fractions; Sect. 3 describes the methodology to correct the inventory based on the measurement–model mismatches. The results are shown in Sect. 4, while Sect. 5 discusses the results and provides conclusions.

2 Measurements and direct simulations

2.1 CO_2 concentration measurements

In this paper, we use CO_2 mole fraction measurements that have been acquired continuously in the framework of the CO_2-Megaparis and ICOS-France projects. Three stations have been equipped with high-precision CO_2/CO analysers (Picarro G1302) specifically for the project objectives. One is located in the heart of Paris, at the summit of the Eiffel Tower, 300 m above the surface. Two are located to the north and north-east of the Paris area in a mixed urban–rural environment. They are complemented by two ICOS-France stations that were operational before the start of the project. One is located in the south-west, about 20 km from the centre of Paris, while the other is a tall tower located further south by about 100 km. Both use gas chromatograph analysers (Agilent HP6890). The locations of the stations are given in Table 1 and are shown in Fig. 1. They are very roughly located along a NE–SW direction, which defines the dominant wind directions, thus favourable for the monitoring of the CO_2 increase due to the emissions of the Paris area, with a station at the edge of the urban area in both directions. The measurements are quality controlled and binned at a temporal resolution of 1 h. They have been regularly calibrated against the WMO mole fraction scale (Zhao and Tans, 2006) so that measurement accuracy to the WMO-X2007 scale is estimated to be better than 0.38 ppm. The instrumental reproducibility is better than 0.17 ppm on the 5 min average measurements available from the CO_2-Megaparis stations, and the temporal averaging to the hourly mean values used in this paper leads to precision much better than the accuracy (Zhao and Tans, 2006).

2.2 Atmospheric transport modelling

Atmospheric transport modelling provides the link between the surface fluxes and the atmospheric mole fractions. Here, we use the Chimere transport model (Menut et al., 2013) with a resolution of 2 km around the city of Paris, and 10 km for the surroundings of the modelling domain (see Fig. 1). There are 118×118 pixels in the modelling grid that covers an area of approximately $500 \times 500\,km^2$. There are 19 layers

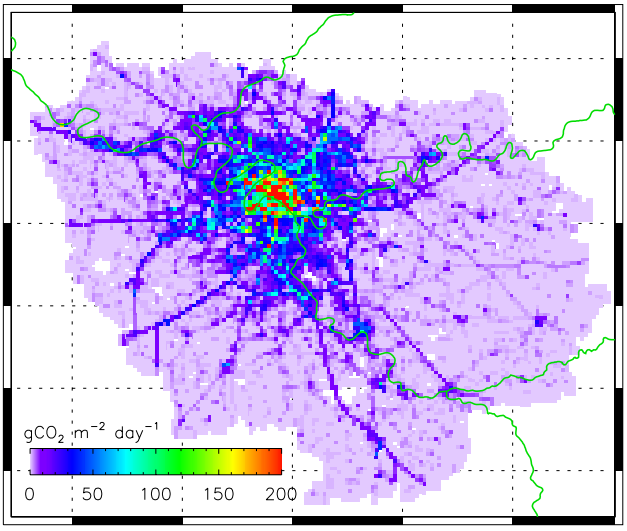

Figure 2. Typical day-total CO_2 emissions of Île-de-France, according to the AirParif year 2008 inventory, for a weekday in October. The point sources are not included in this map. The emissions are provided for the area outlined in red in Fig. 1. The resolution is 1 km. The grid is 0.2° in latitude and 0.4° in longitude.

on the vertical, from the surface to 500 hPa. The Chimere transport model is driven by ECMWF-analysed meteorology at 15 km resolution. There is no urban scheme in the atmospheric modelling that is used here, which may be seen as a significant limitation to our inversion set-up. However, we conducted forward simulation comparisons between our modelling and that used in Lac et al. (2013), which includes specific surface parameterisation to account for the urban area, and we did not find significant differences in the simulated CO_2 mole fractions.

The model simulates the mole fractions that are driven by the surface fluxes and the boundary conditions. The surface fluxes that are accounted for in the simulations are the sum of the following.

- Anthropogenic fossil fuel CO_2 emissions within the Île-de-France region, from the AirParif inventory, as described in Sect. 2.3 and shown in Fig. 2. Île-de-France is the administrative region spreading typically within 60 km around the city of Paris, the boundaries of which are shown in Fig. 1.

- Anthropogenic fossil fuel CO_2 emissions outside the Île-de-France region, according to the Edgar database (Janssens-Maenhout, 2012) available at 10 km resolution. These are only annual mean fluxes, and there is no description of the diurnal or seasonal cycle in this inventory.

- Biogenic fluxes from the C-TESSEL land surface model as described in Sect. 2.4

The CO_2 boundary conditions prescribed at the lateral and top edges of the simulation domain, and transported inside the domain by Chimere, are obtained from the Monitoring Atmospheric Composition and Climate (MACC) global inversion, v10.2 (http://www.copernicus-atmosphere.eu/). In this simulation, the global distribution of surface CO_2 fluxes has been optimised to fit the mole fractions measured at a number of stations distributed over the world, given their assigned uncertainty and prior information of the surface fluxes. Given the relatively coarse spatial resolution of the transport model used in the MACC inversion, CO_2 boundary conditions here are temporally and spatially very smooth and have little impact on the spatial gradients simulated within the domain area.

2.3 AirParif inventory

The AirParif air quality agency (http://www.airparif.asso.fr/en/index/index) has developed an inventory of emissions (for greenhouse gases such as CO_2 but also for air pollutants) at 1 km spatial resolution and an hourly time step for the Île-de-France region. The emissions are quantified by activity sectors. The improvement in methodologies and emission factors leads to frequent updates of the emission estimates.

Nearly 80 different source types are included in the inventory with three main classes: point, linear and diffuse sources. Point sources correspond to large industries, power plants, and waste burning; linear sources are related to transportation, while diffuse sources are mostly associated with the residential and commercial sectors. The road traffic emission estimates use a traffic model and vehicle-counting devices that report the number of vehicles and their average speed over almost 40 000 km portions of roadways. Large industries are requested to report their CO_2 emissions and these are used in the inventory. For smaller industrial sources that are not required to report their emissions, a disaggregation of the regional fuel consumption is made based on the number of employees, leading to larger uncertainties. We have used the latest available version of the inventory, corresponding to the year 2008, which has been developed for five typical months (January, April, July, August, and October) and three typical days (a weekday, Saturday and Sunday) to account for the seasonal and weekly cycles of the emissions. Therefore, this inventory estimates typical emissions but does not attempt to reproduce the daily variations resulting from specific meteorological conditions, or specific events such as public holidays.

Figure 2 shows an example of the spatial distribution of the total emissions for a weekday in October. Typical values are a few hundred $gCO_2\,m^{-2}\,day^{-1}$ within the city and a few tens of $gCO_2\,m^{-2}\,day^{-1}$ in the suburbs. The main roads are clearly shown with flux enhancements of a few tens of $gCO_2\,m^{-2}\,day^{-1}$ at the 1 km^2 resolution of the inventory. Further processing of this map shows that one-third of the

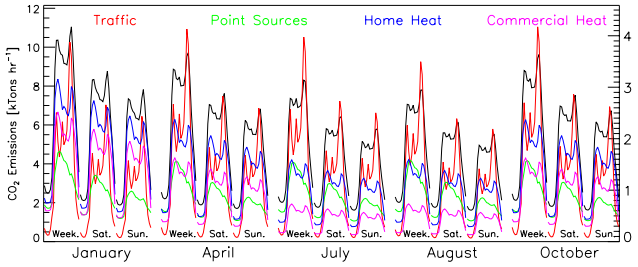

Figure 3. Temporal variation of the main CO_2 emission sectors according to the AirParif inventory for the whole Île-de-France region. The figure shows, for 5 typical months and 3 typical days (weekday, Saturday, Sunday), the hourly CO_2 emissions. The black line is the total emission (left scale), while the four coloured lines are for different sectors (right scale).

Île-de-France emissions are within 10 km of the Paris centre, and that 61 % are within 20 km.

There is a large temporal variation in emissions, as shown in Fig. 3, mostly on the daily scale, but also on the weekly and seasonal scales. Most components show a large daily cycle with minimum emissions at night. During the day, the traffic-related emissions show several maxima in the morning, midday, and late afternoon. The daily cycles of the other activities are less pronounced but nevertheless significant. Point sources have the smallest daily cycle amplitude due to the industrial temporal profile that is relatively flat. The Paris area has few point sources, and they contribute typically 20 % of the total emissions. The seasonal cycle is most pronounced for the residential emissions related to heating and cooking. One notes that residential CO_2 emissions do not go to zero during the summer months, because energy is still consumed for cooking and for heating water in summer.

In the following, the AirParif inventory for the year 2008 is used as a prior estimate of the fossil fuel emissions within the Île-de-France region, both for the direct transport simulations (Sect. 2.5) and for the flux inversion (Sect. 3). Note that the inventory of point source emissions provides injection heights that have been used in the source term of the simulations. The AirParif inventory is provided as a function of legal time, and we have accounted for the time shift between legal time and UTC time, including the impact of daylight saving. Note that, due to the longitude of Paris, UT time and solar times are very similar.

2.4 Biogenic fluxes

The NEE fluxes used here are provided by the land surface component of the ECMWF forecasting system, C-TESSEL (Boussetta et al., 2013). They are extracted from the ECMWF operational archives at the highest available resolutions, 15 km and 3 h. These data are interpolated in space (2 to 10 km) and time (1 h) to be consistent with our atmospheric transport model grid and temporal resolution.

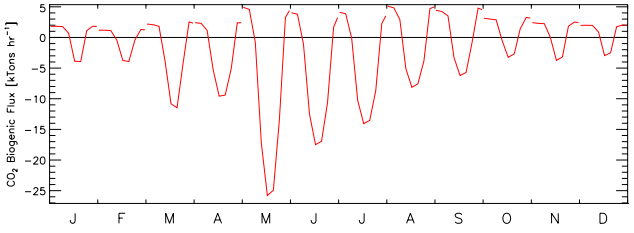

Figure 4. Mean diurnal cycle of the biogenic flux (net ecosystem exchange) for the 12 calendar months and for the same area as in Figs. 2 and 3 which is outlined in red in Fig. 1. The values were derived from an average of the C-Tessel simulations.

Figure 4 shows the mean daily cycle of NEE for the Île-de-France area and for the 12 calendar months. There are large diurnal and seasonal NEE cycles. The flux is positive (emission) during the night and negative (uptake) during the day, even during the winter months, given the rather mild winter temperature prevailing over the Paris area. Nevertheless, the amplitude of the daily cycle of NEE is much larger in summer than it is in winter. The NEE values are of similar magnitude than the anthropogenic emissions with a strong anti-correlation in the daily cycle (negative NEE vs. large anthropogenic emissions during daytime; positive NEE and smaller anthropogenic emissions during the night). During the winter, NEE is relatively small and the anthropogenic emissions clearly dominate, but daytime NEE still offsets on average ~ 20 % of the emissions, according to the C-TESSEL model simulations. During spring and summer, however, the daytime NEE uptake is larger in absolute value than the anthropogenic emissions, as shown through a comparison of Figs. 3 and 4.

As our main interest is in the anthropogenic emissions, we chose to analyse a period when the biogenic flux is small, i.e. during autumn and winter. The present paper focuses on two 30-day periods that start on 21 October and 27 November 2010. During these periods, the monthly mean hourly NEE fluxes are less than $3\,\mathrm{ktCO_2\,h^{-1}}$ over the Île-de-France area. NEE is then small, but not negligible, compared to anthropogenic emissions during the chosen inversion periods.

2.5 Direct CO_2 transport simulations

Figure 5, together with Fig. S1 in the Supplement, shows the time series of the CO_2 mole fractions together with an indication of the modelled wind speed and direction to help the interpretation of the results. These time series are derived from observations and direct atmospheric modelling as described in Sect. 2.2.

The Trainou (TRN) station (bottom row) is far from the Paris agglomeration. In addition, the measurement inlet is 180 m from the surface. It shows a diurnal cycle amplitude that is much smaller than at the other sites. In addition, the modelled contribution from both anthropogenic and biogenic

fluxes within the simulation domains is limited to a few ppm, as shown by the difference between the black and green curves. There are a few exceptions however, essentially when the wind blows from the north, i.e. from the direction of the city of Paris, and transports fossil CO_2 from the urban area to the TRN rural site. The best examples are around 8 and 23 December. For these particular cases, the measurements at TRN are significantly larger than the model results. The underestimate by the model is not limited to these dates and there are significant discrepancies between the model and the measurements at this remote background site, in particular at the end of November and at the beginning of December.

The other sites are much closer to Paris and are then more affected by the fossil CO_2 emissions. At Gif-sur-Yvette (GIF), the largest mole fractions are observed when the wind is from the north-east, which is expected as the city of Paris is in that direction. There is also an impact of the wind, as the largest mole fractions are measured under low wind speed conditions. During the October–November period (Fig. S1), the wind is mostly from the south and south-west, thus not from the city, and there is a relatively good agreement between the modelled and measured mole fractions. In December, the wind direction is more variable, the fossil CO_2 signal appears much larger, and there are very significant differences between the measurements and the model estimates.

Gonesse (GON) is located to the north of the city, while Montgé-en-Goële (MON) is further away, to the north-east. The shorter distance to the main source may explain the larger signal at the former station. The only cases when the modelled anthropogenic contribution is small at GON (small difference between the black and green curves) is when the wind is from the north. For other wind directions, the modelled signal is strong – more than 10 ppm – and there are large differences between the measurements and the modelling results. During December, the measurements are most often larger than the model estimates. A similar observation can be made at MON. Surprisingly, the measurements are significantly larger than the modelling results, even when the wind blows from the north or north-east, i.e. when the Paris agglomeration contribution is negligible (3 December, 6–9 December, 22–23 December). For these cases, the most likely explanation is an underestimate of modelled CO_2 from the boundary conditions or from emissions within the modelling domain outside of Île-de-France. Hereafter, we shall denote this contribution as that from "remote fluxes". Note that this impact from remote fluxes shows a large increase in the mole fraction for the periods discussed above. We may then hypothesise that this increase is underestimated. The interpretation is that anthropogenic emissions from the Benelux area generate high concentrations that are underestimated in the boundary condition field that is used in our simulations.

The EIF site is at the top of the Eiffel Tower, 300 m above the city of Paris. The wind speed for this station is larger than for the other one, simply because it is higher in altitude. One expects atmospheric mixing between the surface emissions and the inlet, so that the measurements are representative of a larger area than e.g. MON and GON. Nevertheless, there are some very significant differences between the modelled and observed mole fractions at EIF. The differences may be huge, larger than 30 ppm, even during the afternoon, e.g on 24 October, 7 November, 3 December, and 12 December. Clearly, our atmospheric modelling framework cannot properly represent the mole fraction time series at the EIF station, either because of strong local (sub-grid-cell) emissions, or because of atmospheric transport processes that are not properly represented, in particular concerning the vertical transport above the city. Further analysis of the model–measurement mismatch is shown in Fig. S3. The largest mismatches are preferentially observed during the morning and for low wind speeds, but are observed at all hours of the day and for all wind speeds and directions, which prevents us from attributing these mismatches to a specific bias in the transport model or to a bias in the estimate of the emissions for a specific area.

The curves in Figs. 5 and S1 show very large temporal variations of CO_2 within a day at all stations. Further analysis confirms that the largest variations are observed during the night, when the mixing layer is shallow. During the night and morning, the atmosphere is often very stable, so that surface emissions accumulate within the lowest atmospheric layers, the thickness of which ranges from a few metres to tens of metres. The atmospheric mole fraction is then mostly sensitive to local fluxes and vertical mixing – an atmospheric process that is difficult to model – so that there is a large uncertainty about the modelled link between the emissions and the atmospheric mole fraction. The nighttime and morning measurements are thus not appropriate for our flux inversion, as inverting them would be too sensitive to atmospheric transport biases. As a consequence, we focus on the concentration measurements acquired during the afternoon only, from noon to 4 p.m., when the mixing layer is usually well developed. The daily averages of these afternoon measured and modelled values are shown in Fig. 5 as diamond symbols.

Figure 6 shows a scatter plot of the measured and modelled mole fractions at the five sites together with the statistics of their comparison. The scatter plots confirm the visual impression of Fig. 5: there is a significant correlation between the measured and modelled mole fractions, which demonstrates the model skill. There are also significant discrepancies and a large bias, in particular at the EIF station. The smallest errors (both biases and standard deviations) are found at TRN, which is the site furthest from Paris.

2.6 Analyses and insight for the inverse modelling configuration

Both the measurements and the modelling results show some impact of the Paris area anthropogenic emissions on the CO_2 mole fractions at the five sites analysed here. The mole frac-

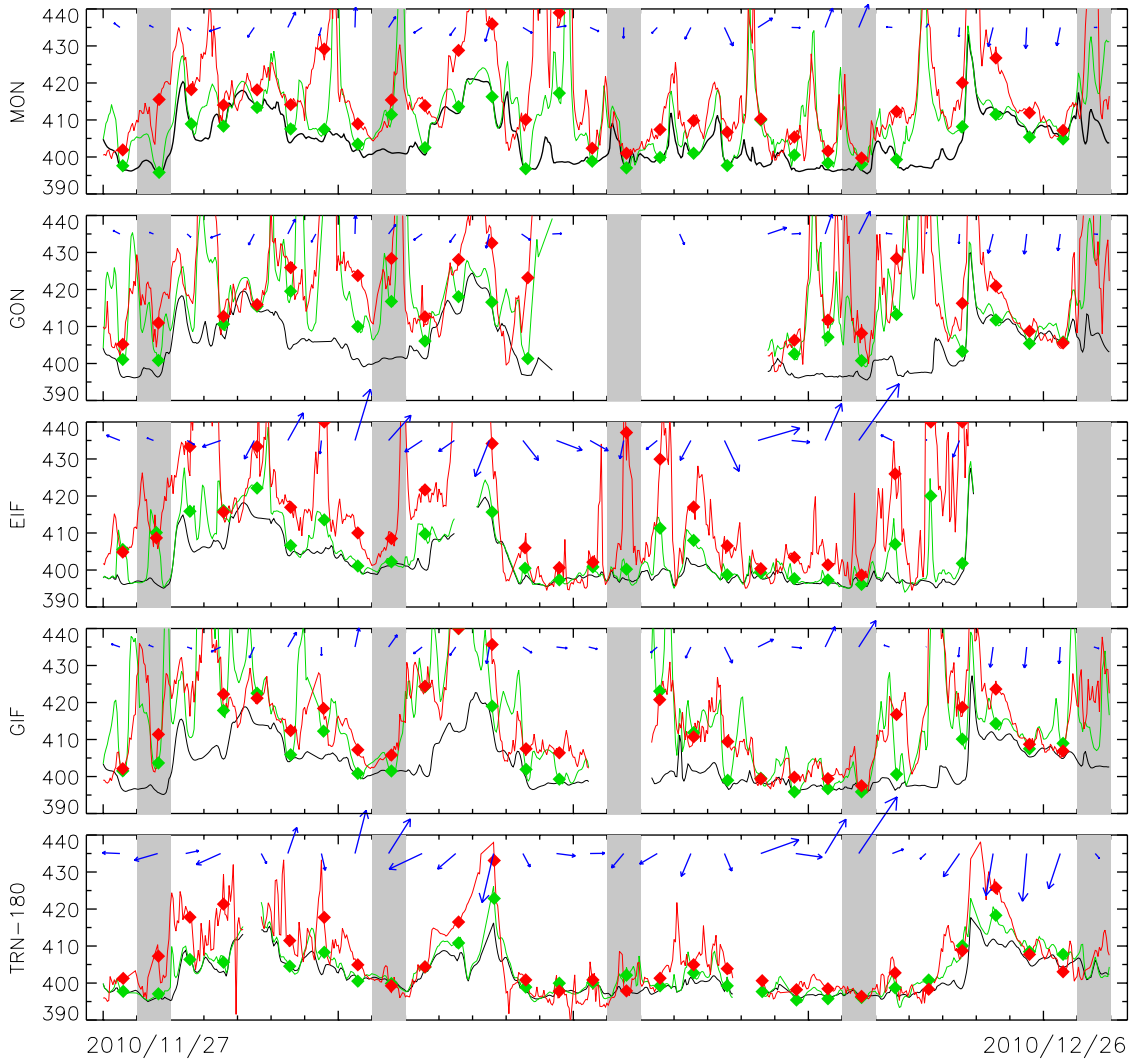

Figure 5. Time series of the measured (red) and modelled (green) CO_2 mole fractions (ppm) for the five sites used in this paper (see Table 1). The black line is the modelled mole fraction that is transported from the domain boundaries, with an additional contribution from anthropogenic emissions outside the Île-de-France region (Edgar fluxes). The green line shows the modelled mole fraction that includes the same contributions, plus the biogenic fluxes within the modelling domain and the anthropogenic emissions within the Île-de-France region. Red are the observations. Note that there are some time periods when no measurements are available due to either calibration processes or, more rarely, failure of the monitoring instrumentation. For such periods, modelling results are not shown. The symbols show the mean of the afternoon measurement–model values that are used for the inversion. The blue arrows indicate the wind speed and direction at noon. A length equivalent to 1 day on the x axis is for a wind speed of $10\,\mathrm{m\,s^{-1}}$. Grey shaded areas indicate Sundays. This figure is for the 30-day period starting on 27 November 2010. Figure S1 in the Supplement shows the same figure for the other period.

tion increases over the modelled large-scale value depend on the wind speed and direction, and a typical order of magnitude is 10 ppm. As expected, the signal is smaller for the rural station of TRN, which is further away from the city than the other sites. Many of the features in the measured time series are well reproduced by the modelling framework, which gives some confidence in its usefulness to improve the emission estimates.

There are also some significant differences between the measured and modelled mole fractions that cannot be justified by inaccurate emission inventories in the Paris area. The most obvious such feature is the mole fraction underestimate at MON and GON under northerly wind conditions when these sites have low sensitivity to the Île-de-France emissions. This feature strongly suggests that remote fluxes lead to mole fraction increases that have biases with typical magnitudes that are similar to the impacts of the Paris area emissions. On the other hand, as the impact from remote fluxes is large scale, one may expect that this impact will be similar for monitoring stations upwind and downwind from the

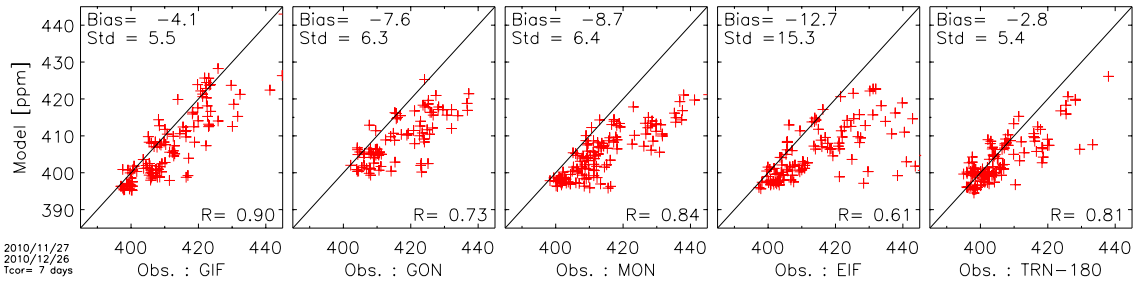

Figure 6. Scatter plot of the measured and modelled CO_2 mole fractions at the five monitoring stations within and in the vicinity of the city of Paris. The model vs. measurement bias, standard deviation and correlations are provided within each subplot. This figure is for the 30-day period starting on 27 November 2010. Figure S2 in the Supplement shows the same figure for the other period.

Paris urban area. The model–measurement error may then be strongly reduced when analysing the difference in mole fractions between two stations that are located upwind and downwind from the Paris urban area, respectively. On the other hand, the mole fraction difference between such stations that are close to the Paris area should contain a clear signature of the emissions from this area, and a relatively weak signature from other fluxes. It then suggests the use of downwind–upwind gradients in the CO_2 mole fractions rather than the absolute value of CO_2 measurements in the inversion procedure.

The other significant feature in the comparison of the modelled and measured CO_2 mole fractions is much larger errors at the EIF site than at the other stations. These results illustrate the difficulty in modelling the CO_2 mole fraction within cities, even with a measurement inlet in altitude, well above the sources. Note that McKain et al. (2012) also find very large (> 30 ppm) model–measurement mismatches within the urban area of Salt Lake City, even when using a high-resolution model. Similarly, Lac et al. (2013) find large model–measurement differences at EIF despite the use of an urban parameterisation in the modelling. The inability to model the CO_2 signal at EIF properly may have a detrimental impact on the emission estimates derived from atmospheric inversion. Conversely, the forward simulations show that the TRN site has low sensitivity to the Paris area emissions due to its location further away from the city than the other sites. Consequently, it cannot be used as a "downwind" site; in addition, GIF is better suited as an "upwind site" for southerly conditions, as it is closer to the urban area and therefore provides better information on the air composition as it enters the city. These features suggest not to use EIF and TRN and rather to focus on MON, GON and GIF to estimate the Paris area emission from their measured mole fractions.

The main objective of the "gradient" inversion method is thus to focus on the monitoring stations that are at the edge of the urban area and to estimate the city-scale emissions by removing most of the upwind signal from the measured and modelled concentrations. The upwind signal is driven by remote fluxes both from the boundary conditions and by fluxes within the model domain but outside the city whose estimates bear very large uncertainties. The inversion method also attempts to select the downwind measurements that are affected by the emissions from a large part of the city, in an attempt to minimise the impact of aggregation errors. Ideally, we would select only the wind direction when one station lies directly downwind from another, with the city of Paris in between. However, given the very limited network of stations surrounding Paris, we have to broaden significantly the range of acceptable wind directions.

Based on this analysis, the emission estimate procedure only uses the measurements from GON, MON and GIF, and is based on the CO_2 mole fraction gradients between the upwind and downwind stations, a method which requires the selection of favourable wind conditions. The mathematical framework is described in the next section, while the inversion results are presented in Sect. 4.

3 Flux inversion

3.1 Principles

We follow a linear Bayesian inversion approach with Gaussian error statistics to determine the optimal surface fluxes (anthropogenic emissions and biogenic fluxes) and their uncertainties from a prior estimate of the fluxes and their uncertainties and from the mole fraction measurements.

We call $\boldsymbol{x}$ the state vector that gathers the scaling factors for the 6-hourly flux maps, $\boldsymbol{x}_\mathrm{B}$ its prior estimate, $\mathbf{H}$ the matrix operator that relates state parameters and mole fraction gradients according to the atmospheric transport model, $\boldsymbol{y}$ the observed mole fraction gradients, $\boldsymbol{y}_\mathrm{F}$ the simulated impact on these mole fraction gradients of the lateral boundary conditions and of the fluxes that are not accounted for in the state vector, $\mathbf{B}$ the uncertainty covariance matrix of $\boldsymbol{x}_\mathrm{B}$, and $\mathbf{R}$ the error covariance matrix of $\boldsymbol{y}$. These components are detailed in the next section.

The optimal solution is given by Tarantola (2005):

$$\boldsymbol{x}_{\mathrm{A}} = \boldsymbol{x}_{\mathrm{B}} + \left(\mathbf{B}^{-1} + \mathbf{H}^{\mathrm{T}}\mathbf{R}^{-1}\mathbf{H}\right)^{-1}\mathbf{H}^{\mathrm{T}}\mathbf{R}^{-1}\left(\boldsymbol{y} - \boldsymbol{y}_{\mathrm{F}} - \mathbf{H}\boldsymbol{x}_{\mathrm{B}}\right) \quad (1)$$

and its posterior error covariance matrix is

$$\mathbf{A} = \left(\mathbf{B}^{-1} + \mathbf{H}^{\mathrm{T}}\mathbf{R}^{-1}\mathbf{H}\right)^{-1}. \quad (2)$$

Note that $\mathbf{B}$ does not depend on the actual measurement values, but varies, among other factors, with their temporal and spatial sampling.

3.2 State vector: $\boldsymbol{x}$

Both the anthropogenic and biogenic prior fluxes described in Sect. 2 show a large diurnal cycle that impacts the model simulations of CO_2, and that is uncertain. It then appears useful to invert this cycle together with the flux daily mean values. However, as discussed earlier, only CO_2 measurements during the early afternoon can reliably be used to estimate the fluxes, and their information about the daily cycle is rather poor. We limit the number of independent periods to four, corresponding to the local times between 0 and 6, 6 and 12, 12 and 18, and 18 and 24 h, respectively.

For the fossil fluxes, we use a scaling factor for each individual day in the state vector, which makes the number of corresponding variables amount to $30 \times 4 = 120$ for the 30-day period of the inversion. These scaling factors apply to the prior flux estimates derived from the AirParif inventory and are denoted λ^i_{0-6}, λ^i_{6-12}, λ^i_{12-18}, λ^i_{18-24}, with i between 1 and 30.

Similarly, we optimise scaling factors of the prior NEE flux from C-TESSEL. The simulation domain shown in Fig. 1 is split into 3×3 large boxes, and we choose the same 6 h periods as for the anthropogenic fluxes to optimise scaling factors of NEE. However, we do not attempt a daily retrieval of NEE, and considered a single scaling factor for optimising monthly NEE for each 6 h window over a 30-day inversion period. The number of variables to optimise NEE is therefore $3 \times 3 \times 4 = 36$. In the following, these NEE scaling factors are shown as α^X_{0-6}, α^X_{6-12}, α^X_{12-18}, α^X_{18-24}, where X is one of the nine large boxes. One of the nine boxes covers the Île-de-France region, while the other ones are in the surrounding area. In the Inversion results sections, we analyse the inversion of NEE for the centre box (X = C) together with those for the anthropogenic emissions. The surrounding boxes provide some ability to the inversion system to control part of the errors from remote NEE, but one cannot expect to get a reliable estimate of the NEE in these areas given the weak observational constraint on this remote NEE.

The state vector $\boldsymbol{x}$ for the linear inversion has therefore $120 + 36 = 156$ variables that represent the scaling factors to the modelled fluxes. The prior value of each of these scaling factors in $\boldsymbol{x}_{\mathrm{B}}$ is 1.

3.3 Measurements gradients: $\boldsymbol{y}$

$\boldsymbol{y}$ contains the measurement gradients that are used to constrain the flux inversion. As explained above, we only use hourly measurements that have been acquired during the afternoon from noon to 4 p.m. local time. In addition, the corresponding measurements need to have a sensitivity to local, unresolved, fluxes that is insignificant in comparison to that of larger-scale fluxes. This condition is not met when the wind speed is low. We therefore use for the inversion only the measurements filtered for wind speeds larger than a given threshold at both sites used to compute the gradient. The results presented in this study are obtained with a threshold of $2\,\mathrm{m\,s^{-1}}$. The wind speed estimate used for such a selection is the one analysed by the ECMWF at the location, height, and time of the observation. This criterion retains about 70 % of the potential measurements.

In Eq. (1), the downwind–upwind differences in mole fraction measurements $\boldsymbol{y}$ are corrected for the contributions that are not accounted for in the state vector ($\boldsymbol{y}_{\mathrm{F}}$). $\boldsymbol{y}_{\mathrm{F}}$ are the modelled mole fractions accounting for the boundary conditions and anthropogenic fluxes outside Île-de-France (prescribed from the Edgar database). This contribution is shown as a blue line in Fig. 5 and Fig. S1 (in the Supplement).

When the wind is from the south-west (upwind direction between 160° and 260°), GIF is considered upwind from the urban area, and the corresponding $\boldsymbol{y}$ elements are the differences between the mole fractions measured at either MON or GON and that measured at GIF. Similarly, when the wind is from the north-east (upwind direction between 0° and 135°), MON is used as an upwind reference to the GIF or GON mole fraction measurements. For other wind directions, the measurements are not assimilated.

3.4 Prior flux uncertainties and error correlations: B

Although we invert the scaling factors of fossil CO_2 emissions for each day and each 6 h period, the uncertainties in these factors are correlated. We therefore attempt to assign correlations for the prior uncertainties based on several considerations: (i) the monthly budget for the AirParif inventory is generally stated to have an uncertainty of 20 %, which is used here; (ii) we assume small positive correlations between the different 6 h windows; (iii) we assume stronger correlations from day to day for a given 6 h window; and (iv) the a priori uncertainty of individual 6 h emissions should have a typical order of 50 %.

Based on these considerations, we set, rather arbitrarily, prior error correlations to 0.4 for two adjacent time periods (e.g. 12–18 and 18–24) and to 0.2 for non-adjacent time periods (e.g. 6–12 and 18–24). For successive days, we use an exponential decorrelation with a characteristic time T_{cor}. The correlation between the prior uncertainties of the fossil CO_2 emission scaling factors is then the product of this exponen-

tial and the time periods' correlation. For instance, the correlation between λ^5_{0-6} and λ^9_{6-12} is $0.4\exp(-4/T_{\rm cor})$.

The results shown in this paper have mostly been obtained with a temporal correlation $T_{\rm cor}$ of 7 days, but other values, from 1 to 30 days, have also been tested. We have verified that such a **B** matrix is positive-definite. The desegregation of the assumed 20 % uncertainty for the monthly emission totals, based on these temporal correlations, results in standard deviations of uncertainties for individual 6 h periods of 33 % ($T_{\rm cor} = 30$ days) to 50 % ($T_{\rm cor} = 7$ days).

For the biogenic flux scaling factors, we set a relative prior uncertainty (standard deviation) close to 0.70 with some variations according to the box size (the variance varies inversely to the surface of the box), based on the numbers derived at 0.5° resolution in Broquet et al. (2011). We do not assign any spatio-temporal correlation between the various biogenic scaling factors, i.e. between the nine boxes or the four time periods. Similarly, there is no correlation in **B** between the prior uncertainties in the biogenic and anthropogenic fluxes.

3.5 Operator matrix: H

The operator matrix **H** provides the link between the surface fluxes and the mole fraction measurements. It combines the spatio-temporal distributions of the fluxes, both for the AirParif inventory and the C-Tessel biogenic fluxes, that are assumed and not modified through the inversion, the atmospheric transport by the Chimere model, the sampling of the atmosphere at the instrument locations, and the selection of gradients according to the criteria developed in Sect. 3.3. Note that the AirParif inventory has a 1 h temporal resolution. The direct simulation ($\mathbf{H}x$) uses the description of the emissions at this temporal resolution. Each element of the state vector corresponds to a natural or anthropogenic surface flux for a longer time period. We use the atmospheric transport model to compute the impact on the mole fraction of each surface flux (156 in total) corresponding to an element of the control vector. The 4-D mole fraction fields from each of these simulations are then sampled at the place and time of the atmospheric observations used to compute the downwind–upwind gradients corresponding to the observation vector. These simulated mole fraction gradients provide the elements of each column of the **H** matrix.

3.6 Observation error: R

The measurements provided by the instrument are precise, certainly better than 0.3 ppm. However, the observation error in **R** also includes any source of misfit between the model and the data that is not accounted for in the state vector, such as the representation error, the impact of the error on the spatial distribution of the fluxes, and the atmospheric transport modelling error. These are difficult to assess (Broquet et al., 2013), although one expects significant values given the very heterogeneous urban environment that is discussed here.

Due to the complexity and misunderstanding of the processes underlying the observation error, which may lead to positive or negative correlations, we ignore observation error correlations in the construction of **R**, which is thus diagonal.

We use two statistical diagnostics of the misfits in the observation space described by Desroziers et al. (2005) to infer typical observation error variances: (i) the agreement between the sum of the uncertainty from the prior estimate of the control parameters and of the observation error with the RMS Root Mean Square of the prior misfits to the assimilated data; and (ii) the agreement between the observation error with the mean of the product of prior and posterior misfits to the assimilated data. Based on this analysis, we set a 3 ppm observation error for the mole fraction gradients that are used for the inversion.

We can note that this value is significantly smaller than the model–measurement differences as shown in Fig. 5. This is due to the fact that the observation errors related to uncertainties in the large-scale impact of the remote fluxes are strongly correlated between the measurement sites at a given time. Therefore, they vanish when considering gradients in the model fractions rather than values at individual sites such as in Fig. 5. This is further discussed in Sect. 4.2.

4 Inversion results

In the following, we present the result of the inversion described in the previous section. We first analyse the modelled mole fractions, prior and posterior, against the measurements. We then analyse the retrieved fluxes, both NEE and fossil fuel.

4.1 Mole fraction gradients

Figures 7 and S4 show the time series of the afternoon-mean mole fraction gradients. Some days are missing, either because either station is unavailable or because the wind direction does not fulfil the selection criteria developed in Sect. 3.3. The prior value is almost always positive, because the reference is chosen upwind of the Paris agglomeration. There are a few exceptions, like on 22 December at GON, MON being used at the upwind reference according to the wind direction. As GON is in the northern part of the Paris agglomeration, one expects a smaller signal than for southerly wind conditions. Further investigation demonstrated that this unexpected behaviour is linked to a large spatial gradient of the CO_2 concentration generated by anthropogenic emissions over the Benelux accounted for in the Edgar inventory and transported by the Chimere model ($\boldsymbol{y}_{\rm F}$ in Eq. 1). Interestingly, the observations confirm the sign and the order of magnitude of the gradient that is modelled with our set-up that uses crude anthropogenic emissions outside Île-de-France.

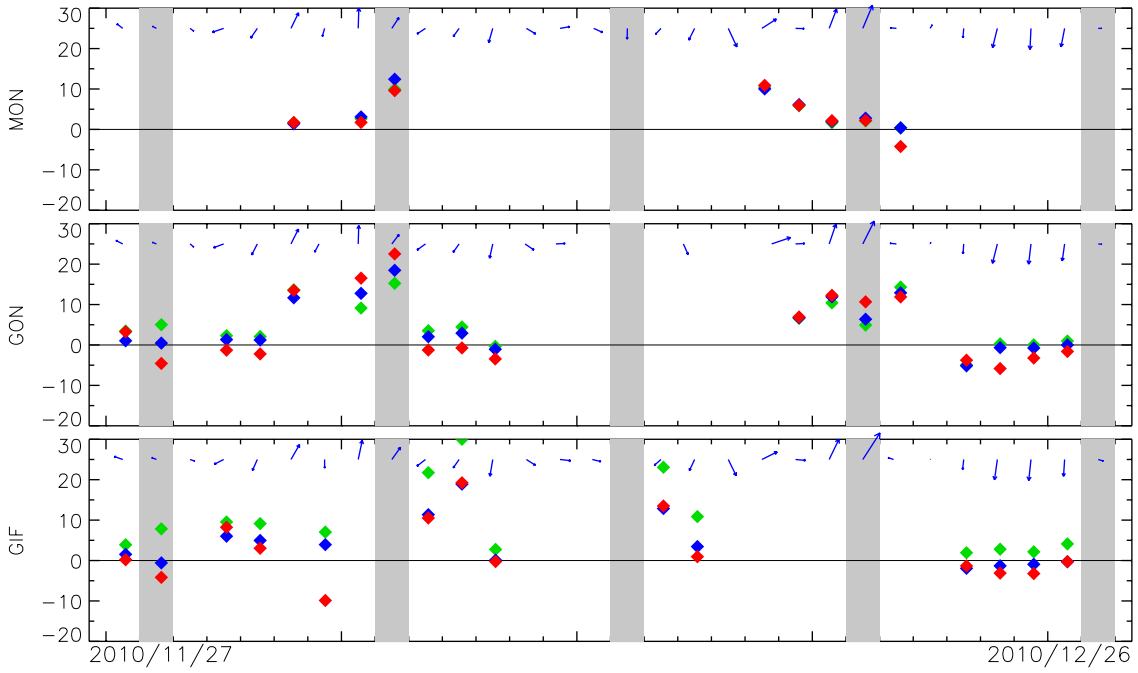

Figure 7. Time series of the mole fraction differences between a station (y axis label) and another one used as a reference (either GIF or GON) and selected based on the wind direction (see Sect. 3.3). The symbols show the mean afternoon concentrations (12 a.m.–4 p.m.) for the measurements (red), and the prior (green) and posterior (blue) estimates. As in Fig. 5, the arrows indicate the wind speed and direction. A similar figure for the other time period is shown in the Supplement.

Another negative gradient is observed at GIF-MON for northerly wind conditions on 3 December. This is very unexpected, and we could not find a valid explanation for this particular case.

In general, the observations are smaller than the prior, and the posterior is in between. Indeed, the inversion result leads to concentration gradients that are closer to the observations. As a result, some of the posterior gradients are negative (see the end of the period at GIF in Fig. 7).

Figures 8 and S4 show scatter plots of measured vs. modelled mole fraction gradients. The first row of the plots in each of these figures shows the modelled mole fractions from the domain boundaries and the fossil CO_2 emission outside Île-de-France (black lines in Fig. 5, $\boldsymbol{y}_F$ in Eq. 1) against the measurement. This constitutes the modelled contribution to the mole fraction that is not optimised by the inversion. The values on the y axis show the modelled impact of the remote fluxes on the upwind–downwind mole fraction gradient. As expected, this impact is small compared to the measured gradient shown on the x axis.

The second row shows simulated CO_2 induced by prior NEE and fossil CO_2 fluxes (i.e. those that are optimised through the inversion) against measured mole fractions corrected for the large-scale values (i.e. $\boldsymbol{y}_F$, shown on the y axis of the first row). Although there is a large spread, the correlation is significant, which shows that the transport model and the prior flux set-up have altogether some ability to reproduce the observed CO_2 mole fraction variability. For the October–November period (in the Supplement), the biases are large for all site gradients (2.1 to 4.8 ppm), whereas, for the November–December period, they are even larger at GIF-MON (7.1 ppm) but rather small in comparison at both other sites. The standard deviation of the measurement–model difference varies with the sites and period, between 2.0 and 5.8 ppm. This is significantly smaller than the standard deviation for the mole fractions (Figs. 6 and S2) that vary between 3.6 and 6.6 ppm. These smaller values confirm the choice made of attempting an inversion based on the mole fraction gradient rather than the individual observations.

After the inversion, the agreement is significantly improved, as shown in the third row. Note however that the standard deviation for the MON site (when GIF is used as a reference) is slightly degraded from the prior value of 2.0 ppm. After the inversion, the correlation between optimised and observed CO_2 gradients for all three stations is larger than 0.90. For the other time period shown in the Supplement (Fig. S5), the correlation statistics are not as good. However, this is due to a lower variability of the gradients, and the posterior standard deviations are 2.3, 2.7 and 2.3 ppm for the three sites, and are then similar to the values shown in Fig. 7.

Overall, the statistics improve significantly between the prior and the posterior, and there is a good agreement between the measured and modelled mole fraction gradients. This raises confidence in our ability to model the impact of

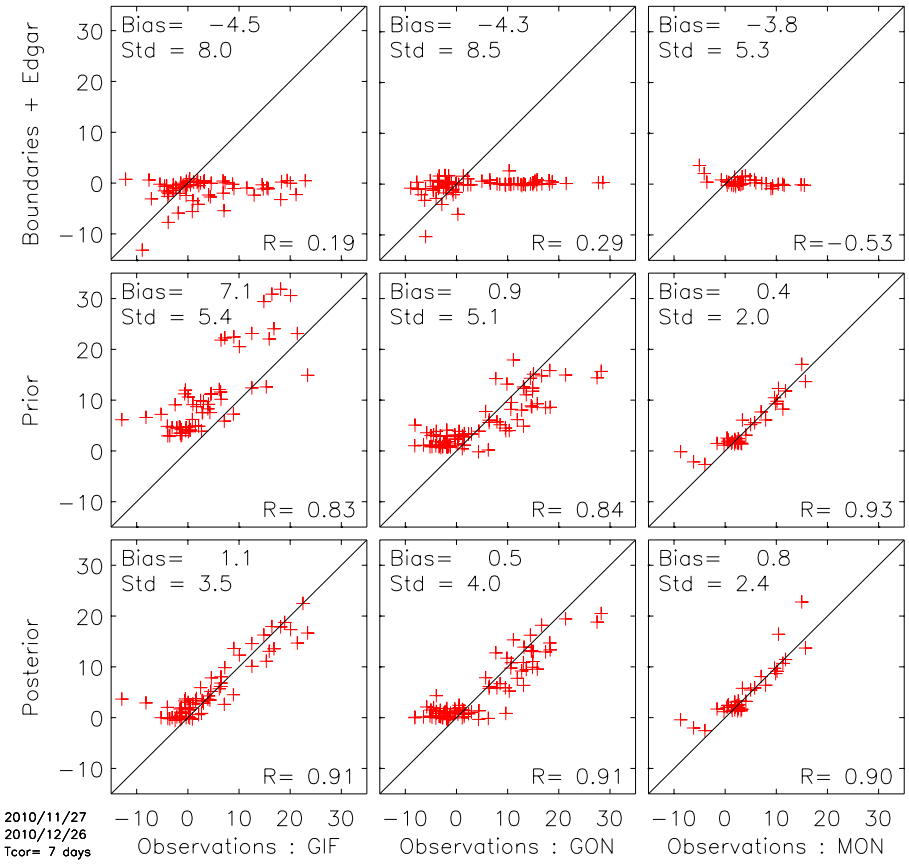

Figure 8. Scatter plot of the measured and modelled concentration gradients for three downwind stations; either GIF or MON is used as an upwind reference. The first row shows the mole fraction simulated using the boundary conditions and the anthropogenic emissions outside Île-de-France ($\boldsymbol{y}_F$ in Eq. 1) against the measurements. The second row shows the concentration estimates derived from the prior values for the biogenic fluxes and anthropogenic fluxes against the corrected measurements (i.e. $\boldsymbol{y}-\boldsymbol{y}_F$ in Eq. 1). The last row is the same but uses the posterior estimates. This figure is for the November–December period. A similar figure for the other time period is shown in the Supplement.

the Paris CO_2 emissions on the atmospheric concentrations for various wind conditions.

4.2 Daily flux estimates

Figure 9 shows the daily anthropogenic fluxes inferred by the inversion procedure. Here, we have aggregated the four 6 h periods as well as their uncertainty, accounting for the error correlations between the periods. Although the inversion controls scaling factors, we show here the resulting fluxes expressed in $MtCO_2$ per day. There is a clear weekly cycle in the prior emissions that are smaller during the weekends. One may also note a shift in prior emission between 29 October and 1 November that corresponds to a change in month and therefore the switch to a different data set in the AirParif inventory. The Airparif inventory includes a profile for October. For November and December, Airparif recommends the use of the January emission profile.

The uncertainty reduction is significant for all the days of the two time periods and a typical order of magnitude is a factor of 2. The emission uncertainty is reduced even for days with no usable measurements, when the wind direction is not within any of the two ranges defined in Sect. 3.3, due to the temporal correlation of the uncertainties and thus of the corrections applied to the prior (Sect. 3.4). The deviations of the flux estimate from the prior follow the gradient observation deviation from the model (see Fig. 7). These deviations are mostly negative, although they are positive for a few days during both time periods. For the November–December period, the posterior emission estimates are within the bounds of the prior uncertainty range. On the other hand, the posterior estimate is much lower than the prior flux during the second half of the October–November period (Fig. 9, top). Interestingly, this period (1 to 20 November 2010) was very mild (MeteoFrance, 2010), which suggests that the heating sector emissions were well below the AirParif inventory values for that period. During this season, according to the AirParif inventory, the heating sector, commercial and residential, amounts to more than 50 % of the emission, so that the total emission is highly sensitive to temperature. Note that

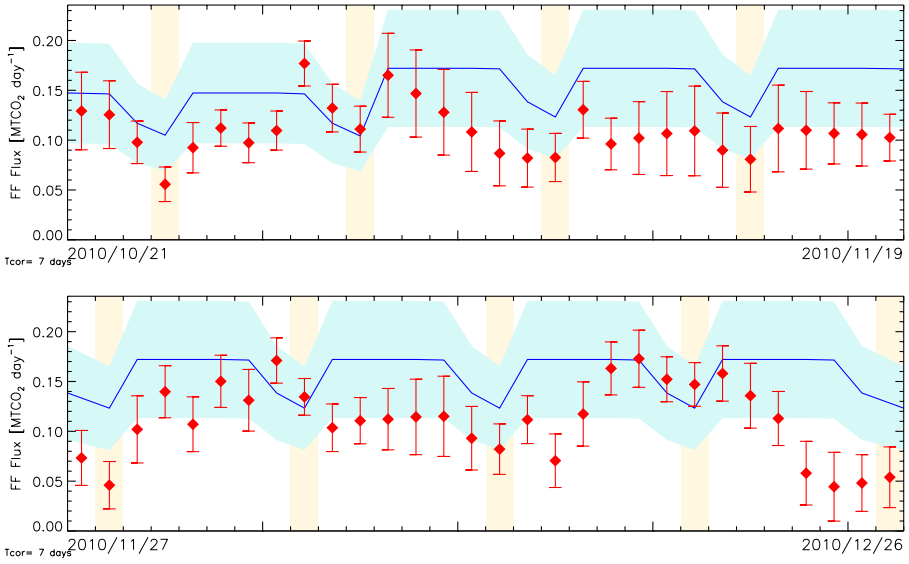

Figure 9. Daily flux estimates of the anthropogenic emission for the 30 days of the period. The blue line and shading show the prior flux according to the AirParif inventory together with its assumed uncertainty. Yellow shading indicates Sundays; note the weekly cycle with lower values during Saturdays and Sundays. The red symbols and bars show the posterior estimates with their uncertainty range. Both 30-day periods are shown.

AirParif recommends the use of the January inventory for both November and December. As the temperatures are generally milder during October than January, one may expect that the inventory will be larger than the true fluxes during October, which is then consistent with the negative correction to the fluxes during that period.

Figure 9 was generated using a 7-day correlation time for the emission uncertainties. We also tested similar inversions using different error correlation times (T_{cor}) in the range of the synoptic to seasonal timescales that drives the emission variability to assess the result sensitivity to this parameter. With a 1-day error correlation time, rather than the 7 days used in our standard configuration, there are days with little or no flux constraint by the observations, while there is no smoothing of the day-to-day variability correction, resulting in an even larger spread of the retrieved fluxes (not shown). At the other extreme, a 30-day correlation time leads to much smoother results. Most of the daily optimised flux estimates remain within the prior uncertainty range.

4.3 Monthly budgets

Figure 10 shows the monthly mean flux estimates for the Île-de-France region for the various 6 h periods. It shows the results of the inversion for the anthropogenic emissions, the NEE of the central box that covers Île-de-France, as well as the total. Note that the total estimate is necessarily the sum of the biogenic and anthropogenic fluxes. Conversely, the uncertainty range of the total is not a simple sum, as it accounts for the correlations between NEE and fossil CO_2 emission errors in the **A** matrix linked to the difficulty in distinguishing NEE and fossil fluxes from the measurements.

The inversion has little impact on the fluxes for the 0–6 h and 18–24 h periods. On the other hand, the impact is strong for the 6–12 h and 12–18 h periods. This is because we only use afternoon observations that are sensitive to the emissions from the morning and afternoon periods only. The assigned correlations in the set-up of the **B** matrix transport some constraint to the other time windows. Although the inversion based on the mole fraction gradients uses few independent observations, because of the additional data selection based on the wind direction, the impact on the flux estimates is significant.

Figure 10 shows that the uncertainty reduction is much larger for the fossil fuel than for the NEE. This is the result of the inversion based on the gradients downwind–upwind from the city which are mostly sensitive to the fluxes in between. The contribution from the NEE to the measurement is then small. Nevertheless, the correlations in the anthropogenic and NEE uncertainties are small (± 0.15 or less). These numbers indicate that the observation sampling provides significant information to distinguish NEE from fossil CO_2 fluxes in the inversion. Although a given measurement cannot trace the origin of the mole fraction excess, the assigned biogenic and anthropogenic flux errors have different spatial and temporal patterns which are exploited by the inversion system to attribute the mole fraction signal to specific sectors. However, this attribution relies on the a priori spatial and temporal distribution of the fluxes that are affected by uncertainties. Thus, the theoretical ability of the system to

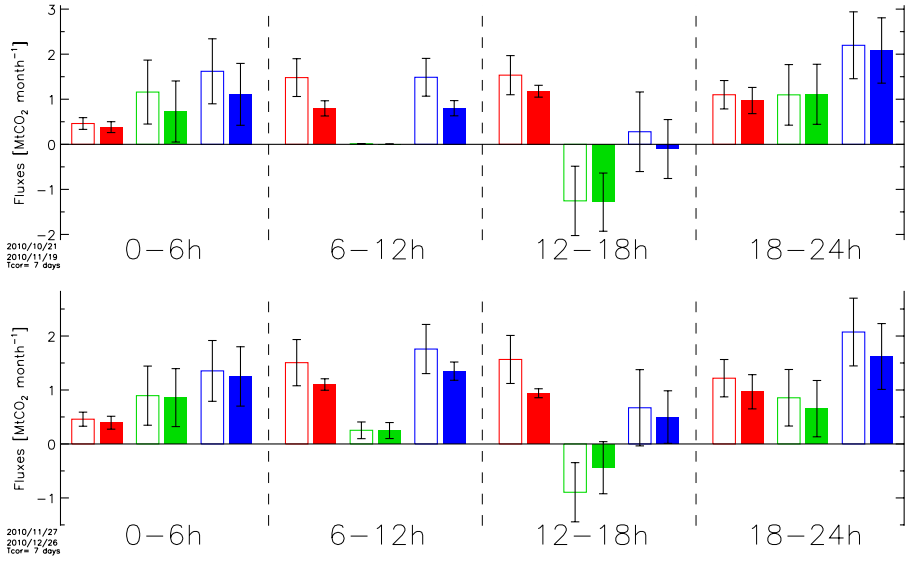

Figure 10. Total flux estimates over the full 30-day period, for the four 6 h periods. Red is for the anthropogenic emissions, green is for the biogenic fluxes, while blue is for the total. The prior estimates are shown as open rectangles, while the posterior is shown as filled rectangles. Both 30-day periods are shown independently.

disentangle natural and anthropogenic fluxes may not be realised in practice.

5 Discussion and conclusions

This paper is a first attempt at estimating the Paris area emissions from measurements of atmospheric CO_2 mole fractions and prior flux knowledge. There is obviously room for improvement in several aspects of the inversion system: the number and spatial distribution of the monitoring stations, the atmospheric transport model including the use of an urban scheme, the modelling of concentrations at the simulation domain boundaries, the definition of the emissions outside Île-de-France, the definition of the control vector, etc. However, first conclusions of broad implications beyond this first attempt can be drawn that should guide further inverse modelling developments for Paris and other cities.

The analysis of the CO_2 time series shows significant differences between the measured and modelled mole fractions upwind of the city of Paris. These differences indicate that the simulated mole fractions at the domain boundaries may be off by several ppm. The errors in this simulation are of similar magnitudes as the signals from the Paris area emissions. Although the number of cases is limited, it seems that the boundary concentrations are significantly underestimated when the wind is from the north or north-east (Benelux). These uncertainties on the domain boundaries generate large-scale errors in the modelled mole fraction and suggest applying the inversion not to the measurements themselves, but rather to upwind–downwind gradients, as was done in this paper. Indeed, the measurement–model agreement is much better for the gradients than it is for the direct values. It confirms that the large-scale pattern of the CO_2 mole fraction, which is not related to the Île-de-France fluxes, is not properly modelled. The information provided by our five-site network does not allow optimisation of the structure of the CO_2 boundary conditions, which is directly prescribed by a coarse-scale global inversion. Exploiting the distant sites currently operational in Europe would be unlikely to improve this situation. In this context, the inversion based upon gradients as presented in Sect. 4 appears necessary. It relies on the assumption that, due to atmospheric diffusion, the signature of remote fluxes upwind of the city is sufficiently homogeneous in space, horizontally and vertically, and time over the path through the city from upwind to downwind sites both located within the afternoon PBL. As a consequence, the main part of such a large-scale signal is removed through the differences between two sites. The validity of this hypothesis is confirmed by the much better agreement between measured and modelled mole fractions as shown through the comparison of Figs. 6 and 8. Both measurements and atmospheric transport simulations indicate, however, that the CO_2 mole fraction signal generated by distant sources outside the Chimere model domain has some spatial structures (see e.g. the variability of modelled values in Fig. 8, top) which need to be accounted for.

The drawback of using the gradient-based inversion method is a reduction in the number of observations, in particular with the current monitoring network that only samples a fraction of possible wind directions. Nevertheless, although the number of observations is very much reduced, our inversion system based on the gradient reports significant uncertainty reductions. It must also be noted that we assumed a

7-day error correlation time for the anthropogenic emissions, so that our system shows flux uncertainty reductions, even on days with no valid observation, as the flux is constrained by observation of the previous or following days.

The setting of temporal error correlation in prior fluxes is therefore essential for the inversion. Although the results in this paper are mostly derived with a 7-day correlation length, this is a somewhat arbitrary choice, and the results are significantly affected when using different values. In particular, a much shorter value (1 day) leads to very large variations in the posterior daily emissions. Further work should be devoted to the assignment of objective correlation lengths based on the processes that lead to emission uncertainties. Climatic conditions in general, and more specifically temperature during the cold season, influence the emission with a timescale that is consistent with synoptic events, i.e. close to a week; the impacts of specific events such as holidays, commemorations or strikes have a much shorter timescale, while inventory biases linked to e.g. the emission factors have an impact on the fluxes on timescales of months or even longer.

Our analysis also indicates model–measurement discrepancies at the EIF site that are much larger than at other sites. On the one hand, this is somewhat surprising, as a measurement inlet at altitude should ensure a larger spatial representativeness than at the surface sites and less sensitivity to local, poorly represented, emissions. Usually, tall tower-based measurements are preferred to those at the surface for the estimate of biogenic fluxes. On the other hand, EIF is located close to the centre of the city of Paris, and is therefore affected by stronger local emissions than the other sites used in this paper. City fluxes are highly heterogeneous, while the model used in this paper has a 2 km spatial resolution, does not include information on the 3-D structure of the urban canopy, and uses limited information on the CO_2 source injection heights. Such a model may then be insufficient to account properly for atmospheric processes that link the local surface fluxes to the concentrations at the top of the Eiffel Tower. Previous results obtained at MeteoFrance by Lac et al. (2013) using a high-resolution (2 km) meteorological model that includes urban parameterisations, and validated against local meteorological measurements, also show high model–data misfits at EIF similar to those found in the present paper. McKain et al. (2012) also show poor skill in representing the mole fraction at urban sites, so that the information content of the measurements is not applied for an estimate of the absolute emissions, but rather for a long-term relative change. These findings can be related to our difficulties in modelling urban CO_2 at EIF using a 2 km resolution transport model that are typical of the current generation of models. The use of urban sites such as EIF for atmospheric inversion will likely necessitate long-term research by the inverse modelling and transport modelling communities.

At present, our mesoscale atmospheric transport model cannot reconcile the measurements at the top of the tower with those at the surface in the vicinity of the city, given our set of surface fluxes and inversion settings. This cast doubts on the quality of the modelling at the other sites. Indeed, if the atmospheric transport model does not properly simulate the atmospheric vertical transport between the surface and an inlet at 300 m in altitude, it likely misrepresents the link between surface fluxes and atmospheric mole fractions. Conversely, the large modelling errors at EIF may be related to its urban location (and to the strong influence of local urban sources), and this would raise concerns regarding the ability to exploit urban measurements, and therefore to solve for the spatial distribution of the fluxes within the urban area.

The largest differences between the measured and modelled concentrations occur for low wind speeds. For this reason, we have chosen a $2\,m\,s^{-1}$ wind speed threshold below which the measurements are not used in the inversion. A larger threshold rejects further observations, and reduces the range of flux corrections through the inversion. The choice of the threshold is somewhat arbitrary and we have refrained from using a large one to clearly demonstrate the impact of a few situations with low wind speed. There are several hypotheses for the poor modelling at low wind speed, including larger representativity errors of subgrid patterns, or larger errors in vertical mixing modelling. However, such issues are continuous and there is no indication that the modelling errors disappear between e.g. 2 and $3\,m\,s^{-1}$. Thus, further rejection of low wind speed observations may hide the deficiencies in the atmospheric transport without improving the flux inversion.

We also stress that our analysis is based on measurements during the late autumn period. This is a favourable case for the inversion of fossil fuel CO_2 emissions, as there is less interference with the biogenic fluxes (Pataki et al., 2007). During spring and summer, the NEE is much larger (in absolute value) and also more uncertain. In fact, during May, the biogenic sink is likely larger than the anthropogenic emissions within Île-de-France, as shown by Figs. 3 and S4. The gradient inversion method is designed also to minimise this interference of biogenic flux with the constraint on anthropogenic fluxes. Indeed, the theoretical posterior uncertainties indicate few correlations between the retrieved NEE and anthropogenic emissions. There is however vegetation within the urban area that may generate a significant sink during the growing season. A successful anthropogenic emission inversion would benefit from additional efforts to describe the biogenic fluxes and the use of additional tracers such as ^{14}C to separate the signature of fossil fluxes and biogenic emissions. One future direction is thus to use a more realistic NEE model over the Paris area that could be calibrated upon local eddy covariance observations (e.g. the method used in Gerbig et al., 2003) and satellite land cover and vegetation activity.

The prior estimate of the Île-de-France CO_2 emissions does not account for human respiration. Yet, within dense urban areas, human respiration can be a significant fraction of the fossil fuel emissions (Ciais et al., 2007; Widory and Javoy, 2003). Respiration by human beings is a source of

CO_2 of typically $1\,kgCO_2\,day^{-1}$ (Prairie and Duarte, 2007), which, assuming a total population of 11.7 million for the Île-de-France, leads to $4.2\,MtCO_2$ per year, or 8 % of the AirParif fossil fuel inventory. Although small, this flux is far from negligible compared to fossil fuel emissions. While the CO_2 mole fraction measurements are sensitive to the human respiration flux, our control vector only accounts for the fossil fuel emissions and NEE fluxes. Although it does not have point sources, the spatial distribution of the human respiration is broadly similar to that of the fossil fuel emissions, so that the inversion will attribute the human respiration mole fraction signal to the fossil fuel rather than to the NEE fluxes. We therefore expect an overestimate of the fossil fuel emission by typically 8 % in our inversion that neglects human respiration. A larger percentage may be expected in summer and a smaller one in winter due to the seasonal cycle of the fossil fuel emissions that has a larger relative amplitude than that of the human respiration. Improvement in our inversion system should explicitly account for the human respiration, based on the spatial distribution of the population.

One often stated objective of the top-down inversion of fossil fuel CO_2 emissions is to provide an independent verification of the bottom-up estimates, i.e. the inventories (Levin et al., 2011; McKain et al., 2012; Duren and Miller, 2012). However, information about the spatial and temporal distribution of the emissions has to be used for inverse modelling to limit aggregation errors in the overall budget. In our case, the number of monitoring stations is far too small to invert the spatial distribution of the emissions independently. We have been able to rely on the comprehensive distribution from AirParif. With a larger number of monitoring stations, it may be possible to estimate some information about the flux spatial distribution, but atmospheric transport is not a reversible process, and some accurate information about the spatial distribution will likely be needed, so that the atmospheric inversion cannot be seen as independent of the inventories, but rather as a means of verifying or refining them. In addition, as long as the accuracy in the atmospheric transport does not allow the use of nighttime or morning measurements, it will not be possible to monitor the daily cycle of the emissions. Thus, the computation of daily or monthly fluxes requires some robust information about the daily cycle that should rely on inventories. Thus, again, our top-down emission estimate is far from being independent of the bottom-up inventory.

Although the inversion procedure provides a posterior uncertainty estimate, one should interpret this uncertainty with caution. Indeed, the mathematical framework used here relies on a number of hypotheses, some of which are crude approximations of the reality, such as the spatial and temporal correlations in the flux uncertainties or the unbiased atmospheric transport modelling. The impact of these assumptions has not been quantified. Although we have no "truth" with which to benchmark the inversion results, and there are not even enough measurement sites to perform "leave-one-out" tests, one can perform some sanity checks on the results. One sanity check is the comparison of the measured and modelled mole fractions (Figs. 8 and S4). The analysis of these figures confirms the ability of our inversion to improve the measurement–model agreement. Nevertheless, we note that the posterior misfit (≈ 2.5 ppm) is still a significant fraction of the signal that is analysed (10–20 ppm). The crucial question is whether the atmospheric modelling error is random or a bias, and we have no element to answer that question. The other sanity check consists in analysing the validity of the retrieved daily fluxes (Fig. 9). In this respect, the daily fluxes show day-to-day variations that are suspicious although not refutable at this stage. A result that points in favour of the flux inversions shown here is the significant reduction from the prior during a period with temperatures above the seasonal normal, and the negative correction of the emissions during November from the prior value that is based on an inventory simulating January emissions. A single such event is certainly not sufficient to validate the inversion system, however. We shall apply the same inversion set-up to more than a year of measurements and analyse the results with respect to the temperature anomaly or another short-term event that may have a significant influence on the Île-de-France CO_2 emissions. More measurement sites are needed to evaluate the skill of the inversion better. The deployment of a network of five sites around Paris within the framework of the CarboCount-City project will help in this direction. In addition, inlets at different altitudes will be installed at the Eiffel Tower station for a better assessment of the CO_2 vertical distribution and transport within the urban area. These will be most useful for the longer-term objective of improving the atmospheric transport modelling within the city, which may allow the EIF measurements to be used by the inversion system.

The Supplement related to this article is available online at doi:10.5194/acp-15-1707-2015-supplement.

Acknowledgements. This study was conducted within the ANR CO_2-Megaparis project and was made possible thanks to funding from the CarboCount and CarboCount-City projects that are co-funded by the Climate KIC programme of the European Institute of Technology. Gregoire Broquet acknowledges funding and support from the Chaire industrielle BridGES, a joint research programme between Thales Alenia Space, Veolia, Université de Versailles Saint Quentin en Yvelines, CEA and CNRS. We thank Lin Wu and Isabelle Pison for assistance as well as all the developers of the AirParif inventory.

Edited by: M. Palm

References

Boussetta, S., Balsamo, G., Beljaars, A., Panareda, A. A., Calvet, J. C., Jacobs, C., van den Hurk, B., Viterbo, P., Lafont, S., Dutra, E., Jarlan, L., Balzarolo, M., Papale, D., and van der Werf, G.: Natural land carbon dioxide exchanges in the ECMWF integrated forecasting system: Implementation and offline validation, J. Geophys. Res.-Atmos., 118, 5923–5946, doi:10.1002/Jgrd.50488, 2013.

Broquet, G., Chevallier, F., Rayner, P., Aulagnier, C., Pison, I., Ramonet, M., Schmidt, M., Vermeulen, A. T., and Ciais, P.: A European summertime CO_2 biogenic flux inversion at mesoscale from continuous in situ mixing ratio measurements, J. Geophys. Res.-Atmos., 116, D23303, doi:10.1029/2011jd016202, 2011.

Broquet, G., Chevallier, F., Bréon, F.-M., Kadygrov, N., Alemanno, M., Apadula, F., Hammer, S., Haszpra, L., Meinhardt, F., Morguí, J. A., Necki, J., Piacentino, S., Ramonet, M., Schmidt, M., Thompson, R. L., Vermeulen, A. T., Yver, C., and Ciais, P.: Regional inversion of CO_2 ecosystem fluxes from atmospheric measurements: reliability of the uncertainty estimates, Atmos. Chem. Phys., 13, 9039–9056, doi:10.5194/acp-13-9039-2013, 2013

Chevallier, F., Ciais, P., Conway, T. J., Aalto, T., Anderson, B. E., Bousquet, P., Brunke, E. G., Ciattaglia, L., Esaki, Y., Frohlich, M., Gomez, A., Gomez-Pelaez, A. J., Haszpra, L., Krummel, P. B., Langenfelds, R. L., Leuenberger, M., Machida, T., Maignan, F., Matsueda, H., Morgui, J. A., Mukai, H., Nakazawa, T., Peylin, P., Ramonet, M., Rivier, L., Sawa, Y., Schmidt, M., Steele, L. P., Vay, S. A., Vermeulen, A. T., Wofsy, S., and Worthy, D.: CO_2 surface fluxes at grid point scale estimated from a global 21 year reanalysis of atmospheric measurements, J. Geophys. Res.-Atmos., 115, D21307, doi:10.1029/2010jd013887, 2010.

Ciais, P., Bousquet, P., Freibauer, A., and Naegler, T.: Horizontal displacement of carbon associated with agriculture and its impacts on atmospheric CO_2, Global. Biogeochem. Cy., 21, Gb2014, doi:10.1029/2006gb002741, 2007.

Desroziers, G., Berre, L., Chapnik, B., and Poli, P.: Diagnosis of observation, background and analysis-error statistics in observation space, Q. J. Roy. Meteor. Soc., 131, 3385–3396, doi:10.1256/Qj.05.108, 2005.

Duren, R. M. and Miller, C. E.: COMMENTARY: Measuring the carbon emissions of megacities, Nat. Clim. Change, 2, 560–562, 2012.

Gerbig, C., Lin, J. C., Wofsy, S. C., Daube, B. C., Andrews, A. E., Stephens, B. B., Bakwin, P. S., and Grainger, C. A.: Toward constraining regional-scale fluxes of CO_2 with atmospheric observations over a continent: 1. Observed spatial variability from airborne platforms, J. Geophys. Res.-Atmos., 108, 4756, doi:10.1029/2002jd003018, 2003.

Gurney, K. R., Law, R. M., Denning, A. S., Rayner, P. J., Baker, D., Bousquet, P., Bruhwiler, L., Chen, Y. H., Ciais, P., Fan, S., Fung, I. Y., Gloor, M., Heimann, M., Higuchi, K., John, J., Maki, T., Maksyutov, S., Masarie, K., Peylin, P., Prather, M., Pak, B. C., Randerson, J., Sarmiento, J., Taguchi, S., Takahashi, T., and Yuen, C. W.: Towards robust regional estimates of CO_2 sources and sinks using atmospheric transport models, Nature, 415, 626–630, doi:10.1038/415626a, 2002.

Gurney, K. R., Razlivanov, I., Song, Y., Zhou, Y. Y., Benes, B., and Abdul-Massih, M.: Quantification of Fossil Fuel CO_2 Emissions on the Building/Street Scale for a Large US City, Environ. Sci. Technol., 46, 12194–12202, doi:10.1021/Es3011282, 2012.

Janssens-Maenhout, G., Dentener, F., Van Aardenne, J., Monni, S., Pagliari, V., Orlandini, L., Klimont, Z., Kurokawa, J., Akimoto, H., Ohara, T., Wankmueller, R., Battye, B., Grano, D., Zuber, A., Keating, T.: EDGAR-HTAP: a Harmonized Gridded Air Pollution Emission Dataset Based on National Inventories. Ispra (Italy): European Commission Publications Office, JRC68434, EUR report No. EUR 25299, 2012, ISBN 978-92-79-23122-0, ISSN 1831–9424, 2012.

Kort, E. A., Frankenberg, C., Miller, C. E., and Oda, T.: Space-based observations of megacity carbon dioxide, Geophys. Res. Lett., 39, L17806, doi:10.1029/2012gl052738, 2012.

Lac, C., Donnelly, R. P., Masson, V., Pal, S., Riette, S., Donier, S., Queguiner, S., Tanguy, G., Ammoura, L., and Xueref-Remy, I.: CO_2 dispersion modelling over Paris region within the CO_2-MEGAPARIS project, Atmos. Chem. Phys., 13, 4941–4961, doi:10.5194/acp-13-4941-2013, 2013.

Lauvaux, T., Pannekoucke, O., Sarrat, C., Chevallier, F., Ciais, P., Noilhan, J., and Rayner, P. J.: Structure of the transport uncertainty in mesoscale inversions of CO_2 sources and sinks using ensemble model simulations, Biogeosciences, 6, 1089–1102, doi:10.5194/bg-6-1089-2009, 2009.

Lauvaux, T., Schuh, A. E., Uliasz, M., Richardson, S., Miles, N., Andrews, A. E., Sweeney, C., Diaz, L. I., Martins, D., Shepson, P. B., and Davis, K. J.: Constraining the CO_2 budget of the corn belt: exploring uncertainties from the assumptions in a mesoscale inverse system, Atmos. Chem. Phys., 12, 337–354, doi:10.5194/acp-12-337-2012, 2012.

Levin, I., Hammer, S., Eichelmann, E., and Vogel, F. R.: Verification of greenhouse gas emission reductions: the prospect of atmospheric monitoring in polluted areas, Philosophical transactions, Series A, Mathematical, physical, and engineering sciences, 369, 1906–1924, 10.1098/rsta.2010.0249, 2011.

Lopez, M., Schmidt, M., Delmotte, M., Colomb, A., Gros, V., Janssen, C., Lehman, S. J., Mondelain, D., Perrussel, O., Ramonet, M., Xueref-Remy, I., and Bousquet, P.: CO, NO_x and $^{13}CO_2$ as tracers for fossil fuel CO_2: results from a pilot study in Paris during winter 2010, Atmos. Chem. Phys., 13, 7343–7358, doi:10.5194/acp-13-7343-2013, 2013.

McKain, K., Wofsy, S. C., Nehrkorn, T., Eluszkiewicz, J., Ehleringer, J. R., and Stephens, B. B.: Assessment of ground-based atmospheric observations for verification of greenhouse gas emissions from an urban region, P. Natl. Acad. Sci. USA, 109, 8423–8428, doi:10.1073/Pnas.1116645109, 2012.

Menut, L., Bessagnet, B., Khvorostyanov, D., Beekmann, M., Blond, N., Colette, A., Coll, I., Curci, G., Foret, G., Hodzic, A., Mailler, S., Meleux, F., Monge, J.-L., Pison, I., Siour, G., Turquety, S., Valari, M., Vautard, R., and Vivanco, M. G.: CHIMERE 2013: a model for regional atmospheric composition modelling, Geosci. Model Dev., 6, 981–1028, doi:10.5194/gmd-6-981-2013, 2013.

MeteoFrance: available at: http://www.meteofrance.fr/climat-passe-et-futur/bilans-climatiques/bilan-2010/bilan-de-lannee-2010#, (last access: 17 February 2015), 2010.

Nehrkorn, T., Henderson, J., Leidner, M., Mountain, M., Eluszkiewicz, J., McKain, K., and Wofsy, S.: WRF Simulations of the Urban Circulation in the Salt Lake City Area for CO_2 Modeling, J. Appl. Meteorol. Clim., 52, 323–340, doi:10.1175/Jamc-D-12-061.1, 2013.

Nordbo, A., Jarvi, L., Haapanala, S., Wood, C. R., and Vesala, T.: Fraction of natural area as main predictor of net CO_2 emissions from cities, Geophys. Res. Lett., 39, L20802, doi:10.1029/2012gl053087, 2012.

Pal, S., Xueref-Remy, I., Ammoura, L., Chazette, P., Gibert, F., Royer, P., Dieudonne, E., Dupont, J. C., Haeffelin, M., Lac, C., Lopez, M., Morille, Y., and Ravetta, F.: Spatio-temporal variability of the atmospheric boundary layer depth over the Paris agglomeration: An assessment of the impact of the urban heat island intensity, Atmos. Environ., 63, 261–275, doi:10.1016/J.Atmosenv.2012.09.046, 2012.

Pataki, D. E., Alig, R. J., Fung, A. S., Golubiewski, N. E., Kennedy, C. A., McPherson, E. G., Nowak, D. J., Pouyat, R. V., and Lankao, P. R.: Urban ecosystems and the North American carbon cycle, Glob. Change Biol., 12, 2092–2102, doi:10.1111/J.1365-2486.2006.01242.X, 2006.

Pataki, D. E., Xu, T., Luo, Y. Q., and Ehleringer, J. R.: Inferring biogenic and anthropogenic carbon dioxide sources across an urban to rural gradient, Oecologia, 152, 307–322, doi:10.1007/S00442-006-0656-0, 2007.

Peylin, P., Rayner, P. J., Bousquet, P., Carouge, C., Hourdin, F., Heinrich, P., Ciais, P., and AEROCARB contributors: Daily CO_2 flux estimates over Europe from continuous atmospheric measurements: 1, inverse methodology, Atmos. Chem. Phys., 5, 3173–3186, doi:10.5194/acp-5-3173-2005, 2005.

Peylin, P., Law, R. M., Gurney, K. R., Chevallier, F., Jacobson, A. R., Maki, T., Niwa, Y., Patra, P. K., Peters, W., Rayner, P. J., Rödenbeck, C., van der Laan-Luijkx, I. T., and Zhang, X.: Global atmospheric carbon budget: results from an ensemble of atmospheric CO_2 inversions, Biogeosciences, 10, 6699–6720, doi:10.5194/bg-10-6699-2013, 2013.

Prairie, Y. T. and Duarte, C. M.: Direct and indirect metabolic CO_2 release by humanity, Biogeosciences, 4, 215–217, doi:10.5194/bg-4-215-2007, 2007.

Tarantola, A.: Inverse problem theory and methods for model parameter estimation, Society for Industrial and Applied Mathematics, Philadelphia, PA, xii, 342 pp., 2005.

Turnbull, J., Sweeney, C., Karion, A., Newberger, T., Tans, P., Lehman, S., Davis, K. J., Miles, N. L., Richardson, S. J., Lauvaux, T., Cambaliza, M. O., Shepson, P., Gurney, K., Patarasuk, R., Zondervan, A.: Towards quantification and source sector identification of fossil fuel CO2 emissions from an urban area: Results from the INFLUX experiment, J. Geophys. Res.-Atmos., 120, 292–312, doi:10.1002/2014JD022555, 2014.

Widory, D. and Javoy, M.: The carbon isotope composition of atmospheric CO_2 in Paris, Earth Planet. Sc. Lett., 215, 289–298, doi:10.1016/S0012-821x(03)00397-2, 2003.

Zhao, C. L. and Tans, P. P.: Estimating uncertainty of the WMO mole fraction scale for carbon dioxide in air, J. Geophys. Res.-Atmos., 111, D08s09, doi:10.1029/2005jd006003, 2006.

Zhao, W., Zhang, N., Sun, J., and Zou, J.: Evaluation and Parameter-Sensitivity Study of a Single-Layer Urban Canopy Model (SLUCM) with Measurements in Nanjing, China, J. Hydrometeorol., 15, 1078–1090. doi:10.1175/JHM-D-13-0129.1, 2014.